The Dynamics of Phase Locking

T. N. KRISHNAMURTI AND D. R. CHAKRABORTY*

Department of Meteorology, The Florida State University, Tallahassee, Florida

(Manuscript received 10 June 2004, in final form 3 January 2005)

ABSTRACT

Many low-frequency phenomena such as the Madden–Julian oscillation (MJO) or the El Niño–Southern Oscillation (ENSO) exhibit rapid growth where they appear to be undergoing a phase locking with other time scales such as the annual cycle. The purpose of this paper is to illustrate an example of phase locking of two different time scales. In this instance it is shown that during such epochs of phase locking a large increase in nonlinear energy exchange occurs from one time scale to the other. This paper utilizes the ECMWF Re-Analysis (ERA-40) datasets for the year 2001 to examine this problem. This study is a sequel to a recent modeling study where the maintenance of the MJO time scale was examined from scale interactions, especially with synoptic-scale waves with ~2–7 day periods. It was shown that a pair of waves on the synoptic time scale can satisfy certain selection rules and undergo triad interactions (kinetic energy to kinetic energy exchanges) and transfer energy. This present study illustrates the fact that during epochs of phase locking such nonlinear interactions can become very large, thus portraying the importance of phase locking. These explosive exchanges are shown from two perspectives: an approach based on kinetic energy exchanges in the frequency domain and another that invokes the boundary layer dynamics in the frequency domain.

1. Introduction

A number of examples have been cited in recent literature on the importance of phase locking among different time scales. These relate to the growth of a low-frequency phenomenon where it comes in phase with other time scales. This paper addresses the uniqueness of this feature from an analytical and computational study from the perspective of nonlinear-scale interactions between different temporal scales of motion. Kim (2002) addressed the phase locking between the biennial and the ENSO time scales. In his study the SST variability on the ENSO time scale was related to the biennial time scale. He noted that numerous El Niño events had different time scales, and the varying duration of the El Niño seems to be related to the phases of the El Niño and the biennial oscillations. Krishnamurti et al. (2000) noted a rapid onset of the 1997 El Niño following its phase locking with a major Madden–Julian oscillation (MJO) event over the Indian Ocean. Such features have also been reported by several other authors. Neelin et al. (2000) found the importance of phase locking of the ENSO and the annual cycle during the onset and termination phase of an ENSO. Ueda's (2002) study on dipole mode in the Indian Ocean concluded that the seasonal difference of the coupling process between the monsoon and the ENSO may be a significant factor for understanding the phase-locking feature of the dipole mode with ENSO. Wang and Xu (1997) worked on climatological intraseasonal oscillations (CISO). Their study reveals that the CISO results from a phase locking of transient intraseasonal oscillations with the annual cycle. Using a modified Cane and Zebiak (1985) model that includes the seasonal variations of the western Pacific wind anomalies and the basic-state thermocline depth, the peaks of La Niña seem to prefer the boreal winter, suggesting that the seasonal variation of the western Pacific surface wind anomalies and the mean thermocline depth are critical factors for the phase locking of the mature La Niña to the boreal winter (An and Wang 2001). Philander et al. (1984) argued that seasonal variations in the position of

* Additional affiliation: Indian Institute of Tropical Meteorology, Pashan, Pune, India.

Corresponding author address: Prof. T. N. Krishnamurti, Department of Meteorology, The Florida State University, Tallahassee, FL 32306-4520.
E-mail: tnk@io.met.fsu.edu

atmospheric heating by the mean wind convergence of the intertropical convergence zone (ITCZ) lead to phase locking of ENSO and the seasonal cycle.

The approach of the present paper is to treat scale interactions in the frequency domain. Pioneering studies in this area of research were first reported by Hayashi (1980) where he provided a framework for such inquiries using energy exchanges as a frame of reference. This was followed up with two applications with global datasets where he showed the nonlinear energy exchanges among different scales of motion (Sheng and Hayashi (1990a,b). They addressed the maintenance of MJO from its interaction with other time scales. They found that the energy exchanges were directed from the synoptic-scale waves to the MJO. Thus we have begun to question the assumption of a notion that synoptic-scale waves are always being excited by the passage of an MJO. In regards to ENSO and the seasonal cycle, one needs to carefully study the energy exchanges in the frequency domain between the ENSO and the annual cycle. Our paper limits itself to the MJO as a centerpiece and does not address the phase locking of ENSO.

In a recent study Krishnamurti et al. (2003) illustrated the maintenance of the MJO from a coupled model simulation. In that study, we used the planetary boundary layer dynamics/thermodynamics of a global coupled model as the frame of reference. This dataset, from the coupled model, was used to investigate the nonlinear triad interactions that were inherent in the surface similarity theory (for the surface fluxes) and in the planetary boundary layer disposition of these fluxes. This work followed the pioneering works of Businger et al. (1971) and Louis (1979). We noted a marked increase in the flux of latent heat across the PBL on the time scale of the MJO in the model datasets. That sequential increase in the moisture flux from the surface layer to the top of the planetary boundary layer was examined in the context of scale interactions. It was possible to show that the large growth of fluxes on the time scale of the MJO arose from interactions of MJO time scale frequencies with pairs of frequencies on the synoptic time scale (2–7 days). There was a rich triad of frequencies that satisfied what were called trigonometric selection rules for the interactions to occur and to amplify (or weaken) the MJO time scale fluxes of moisture. Results, especially those from the western Pacific Ocean and the Indian Ocean, suggested this strong possibility for the enhancement of the MJO time scale. That paper also conveyed some information on the tropospheric expanse of the MJO time scale via deep convection and related large planetary-scale divergent circulations. In the course of examining those coupled model–generated datasets, we noted enhancements of these interactions (among the MJO time scale and the synoptic time scale) occurred during episodes of phase locking.

The purpose of this short paper is to elucidate the nonlinear dynamics of this feature. The present study makes use of the European Centre for Medium-Range Weather Forecasts (ECMWF) reanalysis datasets. In this study we shall examine epochs of large growths of eddy kinetic energy and of moisture fluxes on the time scale of the MJO during episodes of phase locking. This paper takes a hard look at the phase locking of the MJO with respect to the synoptic scale and the related consequences. In particular we wish to explore scale interactions among frequencies (MJO and the synoptic scale) and their settings during phase locking to illustrate how such a feature can lead to possible explosive growth of a time scale. Both of these avenues of inquiry (energetics and PBL fluxes) entail triple-product nonlinearities that are described by triad interactions. Such interactions are central to the communication of information among different frequencies.

The aforementioned triad interactions in the for mulation of energetics are essentially transfers of kinetic energy to kinetic energy among different scales. That needs to be contrasted with quadratic nonlinearities, such as those that one encounters in the generation of available potential energy (a covariance of heating and temperature, i.e., quadratic) or the conversion of eddy available potential energy to eddy kinetic energy (a covariance of vertical velocity and temperature, i.e., quadratic). These are in-scale (single scale) interactions.

When we examine a time series of a single variable (such as the zonal wind at the 850-hPa level) at a single location we can illustrate the "in and out" of phase behavior of long and short time scales. Those can, in principle, interact through nonlinear dynamics. Figure 1 shows a superposition of all waves on the time scale of 30–60 days (combined) with those of all waves on the time scale of 2–7 days. The Butterworth bandpass filter is applied for this purpose. Here we do see occasional phase locking among this family of low- and high-frequency motions. In this illustration this seems to occur around days 130 and 153. Days are labeled along the abscissa. Here day 1 corresponds to 1200 UTC 1 April 2001. The ordinate in Fig. 1 denotes the bandpass-filtered zonal wind in units of meters per second. In this paper we show that nonlinear energy exchanges can amplify when phase locking occurs among families

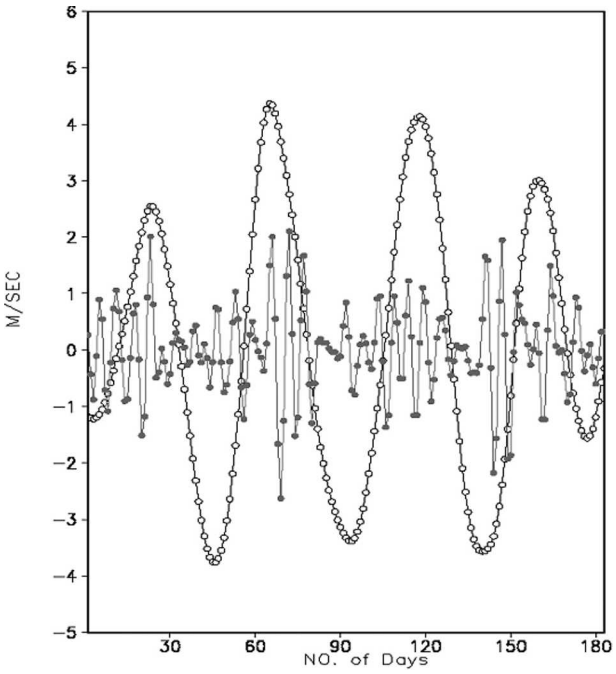

FIG. 1. Superposition of waves on the time scale of 30–60 days (combined) in the zonal wind with those of all waves on the time scale of 2–7 days (combined) at 850 hPa for the period between Apr and Sep 2001 (180 days).

of waves on two disparate time scales. This kind of phase locking can occur a few times during the year.

2. Datasets

Our analysis is based on the 40-yr ECMWF Re-Analysis (ERA-40). This analysis is provided to the user community at a horizontal resolution of 2.5° latitude–longitude at 27 vertical levels. We have used daily analysis covering a period from April 2001 to September 2001. The following variables were available in this reanalysis dataset: wind components (u, v), vertical velocity (w), temperature (T), relative humidity (rh), and geopotential height (Z). We have also accessed the ERA-40-based archive of the surface and planetary boundary layer fluxes of heat, moisture, and momentum on a daily basis. This is a global dataset. The variables that might be relevant for the nonlinear phase-locking mechanism of the MJO could include winds, temperature, bulk coefficients, and humidity in the lower atmosphere and the sea surface temperatures. A temporal Fourier decomposition is employed in order to separate the high-frequency transients and the low-frequency transients from the daily total values of these variables. Furthermore, area averaging is carried out over the following three domains where prominent activity of MJO was previously noted by Krishnamurti et al. (2003):

1) Indian monsoon domain: 10°S–10°N, 60°–110°E
2) Western Pacific Ocean (warm pool): 10°S–10°N, 150°–130°E
3) Central Pacific Ocean: 10°S–10°N, 160°W–180°

The database was next used for the construction of frequency cospectra and cross bispectra in terms of the amplitudes and phases of the participating triads in nonlinear interactions following our previous study (Krishnamurti et al. 2003).

3. Formulation for computing nonlinear phase locking through triad interactions

To address the phase-locking issue we use two different mathematical formulations that invoke scale interactions among three frequencies. The first of these is a problem of kinetic energy exchanges between a frequency in the MJO time scale, n, with two near-adjacent frequencies, r and s, on the synoptic scale. It should be noted that we work with a wide window where the MJO spans 30–60 days and the synoptic-scale waves cover 2–7 days. We take into account all possible triads within these windows and perform an averaging after a consideration of all permissible limits. The frequencies satisfy the so-called trigonometric selection rules following Krishnamurti et al. (2000):

$$n = r + s$$

$$\text{or} \quad n = |r - s|.$$

Kinetic energy to kinetic energy exchanges that involve the triple product and call for interactions are worth examining for the phase locking among different frequencies. The second approach that we address here is the fluxes of moisture, sensible heat, and momentum using surface similarity theory and a planetary boundary layer algorithm. These are discussed in some detail in our recent paper (Krishnamurti et al. 2003). In this study we show that these surface flux computations explicitly carry triple-product nonlinearities and have a very similar triad interaction structure in the frequency domain. What we had noted in our previous study (Krishnamurti et al. 2003) was that fluxes of moisture on the time scale of the MJO amplify successively as we proceed from the ocean surface to the top of the PBL. This occurs largely from scale interactions among the MJO frequencies and the synoptic-scale frequencies. This provides the enhancement of the MJO fluxes via triad interactions. Since a triplet of frequencies was involved in this growth of the MJO time scale (Krishna-

murti et al. 2003), we felt that a closer examination of the phase-locking epochs and their relationship to the scale interactions and fluxes was worth examining. The mathematical formulations of the kinetic energy interactions and surface layer/PBL flux are given in the appendix.

4. An interpretation of kinetic energy exchanges among frequencies ν_1, ν_2, and ν_3 during phase locking

To examine the phase-locking aspect, the cosine and sine coefficients of the variables in Eqs. (A3) and (A4) can be considered in terms of the amplitudes and phase angles of the respective variables. For example, the terms RIC(n) and RIS(n) appearing in Eq. (A4) can be written for one component as

$$\mathrm{RIC}(n) = A_n^{\mathrm{RI}} \cos\theta_n^{\mathrm{RI}},$$

$$\mathrm{RIS}(n) = -A_n^{\mathrm{RI}} \sin\theta_n^{\mathrm{RI}},$$

$$\text{where} \quad A_n^{\mathrm{RI}} = [\mathrm{RIC}^2(n) + \mathrm{RIS}^2(n)]^{1/2}$$

$$\text{and} \quad \theta_n^{\mathrm{RI}} = \tan^{-1}\left[-\frac{\mathrm{RIS}(n)}{\mathrm{RIC}(n)}\right].$$

For purposes of illustration and elucidation we have, here, selected a salient term from the kinetic energy exchanges in the form of transfer of energy into frequency n by interaction among different frequencies excluding 0. Computations using all of the terms (Krishnamurti et al. 2003) suggested that the following was one of the most important terms in the scale interactions:

$$\begin{aligned}\langle L(n)\rangle = {} & \frac{1}{2}\left[\begin{array}{c} -\sum\limits_{r+s=n} \\ -\sum\limits_{r-s=n} \\ -\sum\limits_{r-s=-n} \end{array}\right] \mathrm{UOC}_n\mathrm{UTC}_r \times \left[\left(2\frac{\partial \mathrm{UTC}_s}{\partial x} + \frac{\partial \mathrm{VTC}_s}{\partial y}\right)\right] + \frac{1}{2}\left[\begin{array}{c} -\sum\limits_{r+s=n} \\ -\sum\limits_{r-s=n} \\ +\sum\limits_{r-s=-n} \end{array}\right] \mathrm{UOS}_n\mathrm{UTS}_r \\ & \times \left[\left(2\frac{\partial \mathrm{UTC}_s}{\partial x} + \frac{\partial \mathrm{VTC}_s}{\partial y}\right)\right] + \frac{1}{2}\left[\begin{array}{c} +\sum\limits_{r+s=n} \\ -\sum\limits_{r-s=n} \\ -\sum\limits_{r-s=-n} \end{array}\right] \mathrm{UOC}_n\mathrm{UTS}_r \times \left[\left(2\frac{\partial \mathrm{UTS}_s}{\partial x} + \frac{\partial \mathrm{VTS}_s}{\partial y}\right)\right] \\ & + \frac{1}{2}\left[\begin{array}{c} -\sum\limits_{r+s=n} \\ +\sum\limits_{r-s=n} \\ -\sum\limits_{r-s=-n} \end{array}\right] \mathrm{UOS}_n\mathrm{UTC}_r \times \left[\left(2\frac{\partial \mathrm{UTS}_s}{\partial x} + \frac{\partial \mathrm{VTS}_s}{\partial y}\right)\right], \end{aligned} \tag{1}$$

where the cosine and sine coefficients can be considered in terms of the amplitudes and phase angles of the respective variables, although we have selected only the lead term of the scale interaction in Eq. (A1) the following analysis does apply to each and every term since their structure is very similar.

a. A simple trigonometric illustration

Here we shall take the single term from the above summation and provide a simple trigonometric illustration of phase locking. For example, the terms UTC_r and UTS_r appearing in the above equation can be written as

$$\mathrm{UTC}_r = A_r^{\mathrm{UT}} \mathrm{Cos}\theta_r^{\mathrm{UT}},$$

$$\mathrm{UTS}_r = -A_r^{\mathrm{UT}} \mathrm{Sin}\theta_r^{\mathrm{UT}},$$

$$\text{where} \quad A_r^{\mathrm{UT}} = (\mathrm{UTC}_r^2 + \mathrm{UTS}_r^2)^{1/2}$$

$$\text{and} \quad \theta_r^{\mathrm{UT}} = \tan^{-1}\left(-\frac{\mathrm{UTS}_r}{\mathrm{UTC}_r}\right).$$

This introduces the phase angle θ_r^{UT}, where r is a frequency. Each of the frequencies is thus assigned a phase angle. Thus, all the terms in Eq. (1) are expressed in terms of amplitudes and phases of the relevant frequencies. The special case of phase locking is where the

phases of the three frequencies are all identical. We can examine this energy exchange in the context of different phases for a triad of frequencies. From the above equation we can estimate the consequences of phase locking. Here three frequencies of the flow fields ν_2 and ν_3 interact in such a way as to contribute to the increase (or decrease) of a frequency ν_1. These are subject to the selection rule:

$$\nu_1 = \nu_2 + \nu_3$$
$$\text{or} \quad \nu_1 = |\nu_2 - \nu_3|.$$

We shall illustrate some examples of this energy exchange as a function of different phases for the three interacting frequencies. In Figs. 2a–f we have selected different possibilities. Figure 2a is a very special case where we can examine what happens when all three frequencies carry the same phases. Along the abscissa and the ordinate we have the phases for two frequencies υ_1 and υ_2, respectively. Along a principal diagonal of this illustration the phases of υ_1 and υ_2 are identical. The computation of the energy exchange is done with respect to a third frequency, υ_3, for the special case where its phase is set identical to those of υ_2 always. Here two high frequencies, υ_2 and υ_3, always carry the same phase. The results of computations of energy exchange for the growth of energy of a low frequency, υ_1, when it interacts with two higher frequencies, υ_2 and υ_3, are shown in this diagram. This special case resides along the principal right diagonal along which the phases of υ_1, υ_2, and υ_3 are the same. We note that a maximum of energy exchange does reside along this principal diagonal. The values of energy exchanges, away from the principal diagonal are smaller where the phases of υ_1 and υ_2–υ_3 are different.

In a qualitative manner we can explain how such a phase locking among three wave components leads to maximization of the energy growth for one of the waves. Here we have taken a further idealized simple trigonometric representation for the three wave components.

In Eq. (A5) of the nonlinear energy transfer let us consider the term

$$\begin{aligned}
&\mathrm{UOS}_n \times \mathrm{UTS}_r \times 2\frac{\partial}{\partial x}\mathrm{UTC}_s \\
&= 2(A_n^{\mathrm{UO}} \sin\theta_n^{\mathrm{UO}} \times A_r^{\mathrm{UT}} \sin\theta_r^{\mathrm{UT}} \\
&\quad \times A_s^{(\partial/\partial x)\mathrm{UT}} \times \cos\theta_s^{(\partial/\partial x)\mathrm{UT}}) \\
&= 2A_n^{\mathrm{UO}} A_r^{\mathrm{UT}} A_s^{(\partial/\partial x)\mathrm{UT}} \sin\theta_n^{\mathrm{UO}} \sin\theta_r^{\mathrm{UT}} \cos\theta_s^{(\partial/\partial x)\mathrm{UT}} \\
&= A_n^{\mathrm{UO}} A_r^{\mathrm{UT}} A_s^{(\partial/\partial x)\mathrm{UT}} \sin A \sin B \cos B \\
&= A_n^{\mathrm{UO}} A_r^{\mathrm{UT}} A_s^{(\partial/\partial x)\mathrm{UT}} [\cos(A - B) - \cos(A + B)] \cos B,
\end{aligned} \tag{2}$$

where A_f^X and θ_f^X are the amplitude and phase angle of the variable, X, associated with frequency, f, respectively and are expressed as

$$A_f^X = (\mathrm{XC}_f^2 + \mathrm{XS}_f^2) \quad \text{and} \quad \theta_f^X = \tan^{-1}\left(-\frac{\mathrm{XS}_f}{\mathrm{XC}_f}\right),$$

where XC_f and XS_f are the cosine and sine coefficients of the variable X.

It is further assumed that the phase angle of low-frequency wave $\theta_n^{\mathrm{UO}} = A$ and those of high-frequency waves have equal-phase angles and thus can be written as

$$\theta_r^{\mathrm{UT}} = \theta_s^{(\partial/\partial x)\mathrm{UT}} = B.$$

It can be concluded qualitatively from Eq. (2) that to have maximum transfer of energy into the low-frequency wave having phase angle A due to its interactions with the high frequencies having equal-phase angles B, one important possibility could be $\cos(A - B) = 1 = \cos 0$, which means $A = B$, which would illustrate phase locking.

Let us consider another term in Eq. (1) and evaluate it in a way similar as before:

$$\begin{aligned}
&\mathrm{UOC}_n \times \mathrm{UTS}_r \times 2\frac{\partial}{\partial x}\mathrm{UTS}_s \\
&= 2(A_n^{\mathrm{UO}} \cos\theta_n^{\mathrm{UO}} \times A_r^{\mathrm{UT}} \sin\theta_r^{\mathrm{UT}} \times A_s^{(\partial/\partial x)\mathrm{UT}} \\
&\quad \times \sin\theta_s^{(\partial/\partial x)\mathrm{UT}}) \\
&= 2A_n^{\mathrm{UO}} A_r^{\mathrm{UT}} A_s^{(\partial/\partial x)\mathrm{UT}} \cos\theta_n^{\mathrm{UO}} \sin\theta_r^{\mathrm{UT}} \sin\theta_s^{(\partial/\partial x)\mathrm{UT}} \\
&= 2A_n^{\mathrm{UO}} A_r^{\mathrm{UT}} A_s^{(\partial/\partial x)\mathrm{UT}} \cos A \sin B \sin B \\
&= A_n^{\mathrm{UO}} A_r^{\mathrm{UT}} A_s^{(\partial/\partial x)\mathrm{UT}} [\sin(A + B) - \sin(A - B)] \sin B.
\end{aligned} \tag{3}$$

Again from the above equation, it is seen qualitatively that one important condition for maximum transfer of energy to the low frequency, n, with phase angle A in its interaction with the high frequencies having equal-phase angles B, is $\sin(A - B) = 0 = \sin 0$, which implies $A = B$.

We shall next consider the term,

$$\begin{aligned}
&\mathrm{UOS}_n \times \mathrm{UTC}_r \times 2\frac{\partial}{\partial x}\mathrm{UTS}_s \\
&= 2(A_n^{\mathrm{UO}} \sin\theta_n^{\mathrm{UO}} \times A_r^{\mathrm{UT}} \cos\theta_r^{\mathrm{UT}} \times A_s^{(\partial/\partial x)\mathrm{UT}} \\
&\quad \times \sin\theta_s^{(\partial/\partial x)\mathrm{UT}}) \\
&= 2A_n^{\mathrm{UO}} A_r^{\mathrm{UT}} A_s^{(\partial/\partial x)\mathrm{UT}} \sin\theta_n^{\mathrm{UO}} \cos\theta_r^{\mathrm{UT}} \sin\theta_s^{(\partial/\partial x)\mathrm{UT}} \\
&= 2A_n^{\mathrm{UO}} A_r^{\mathrm{UT}} A_s^{(\partial/\partial x)\mathrm{UT}} \sin A \cos B \sin B \\
&= A_n^{\mathrm{UO}} A_r^{\mathrm{UT}} A_s^{(\partial/\partial x)\mathrm{UT}} [\sin(A + B) + \sin(A - B)] \cos B.
\end{aligned} \tag{4}$$

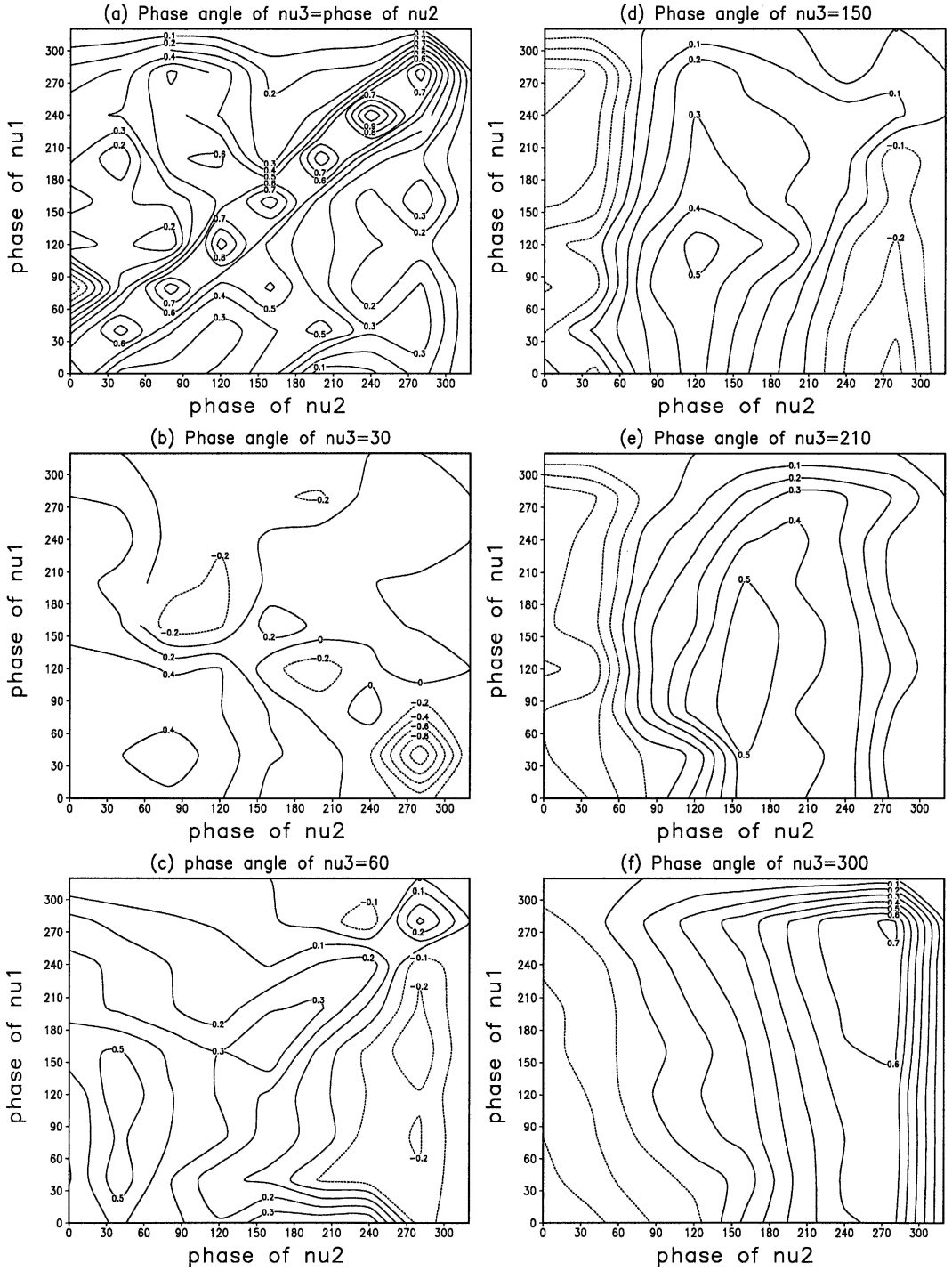

FIG. 2. (a) Kinetic energy (KE) exchanges in the units of W kg^{-1} among low frequency, ν_1, and high frequencies $\nu_2 - \nu_3$, motions when phase angle of ν_2 = phase angle of ν_3 . (b)–(f) Same as (a) but for phase angles of 30°, 60°, 150°, 210°, and 300°, respectively.

In the situation of phase locking (i.e., $A = B$), $\sin(A - B) = 0$: $A = \pi/4$ can maximize this function since $\cos\pi/4 = 1/(2)^{1/2}$. This can be a situation of phase locking where two of the synoptic scales have the same phase B; the MJO is phase locked with the synoptic-scale phase B (i.e., A = B).

In the other panels in Fig. 2 we show several examples of energy exchanges among ν_1, ν_2, and ν_3 where

the phase angle of ν_3 was set to a fixed value and those of ν_1 and $\nu_2$were permitted to vary. In these illustrations a large maximum of energy exchanges greater than 0.8 $\times 10^{-7}$ W kg^{-1} was not seen (as was evident for the phase-locking case, Fig. 2a). In these illustrations we can still select individual points where the phases of ν_1, ν_2, and ν_3 happen to be identical; we note that at those locations a maximum energy exchange does seem to reside in that vicinity. These computations illustrate that the salient term in the scale interaction among a triad of frequencies does seem to maximize when their phases are identical.

The above examples were provided merely to illustrate the possibility of maximum energy exchanges during phase locking from individual terms.

b. *What do full energy exchange computations reveal about phase locking?*

We shall next address the same issue using the complete kinetic to kinetic energy exchange equations. Since we are addressing interactions among different frequencies, it was not necessary to examine the thermodynamical components since they involve quadratic products ($H'T'$, $-\varpi'T'/p$) that are inherently "in-scale" conversion. The nonlinear phase-locking event that we are concerned with in the present study deals with the presence of more than one scale of temporal oscillation. This is the very basis of the phase-locking phenomena.

An and Jin (2004) emphasized $-\varpi'(\partial T'/\partial z)$, which is indeed included in our complete treatment of the nonlinear energetics arising from the advective terms. Their term needs to be multiplied by T' in order to make it one of the terms of our available potential energy equation and this thus becomes a triad. Jin's term comes from first law and is quadratic, ours comes from the available potential energy and the same term becomes a triad.

In this section we shall present some results of kinetic energy exchanges that arise from interactions among triplets of frequencies (Sheng and Hayashi 1990a,b; Krishnamurti et al. 2000; Chakraborty and Agarwal 1996). Equation (A1) was applied to these datasets (described in section 2) at the 850- and the 1000-hPa levels. Computations were done for the following two categories:

1) Loss or gain of kinetic energy for the MJO time scales (30–60 days) when it interacts with all permissible pairs of scales.
2) Loss or gain of kinetic energy for the MJO time scale (30–60 days) when it interacts with the synoptic time scales (here defined as 2–7 days).

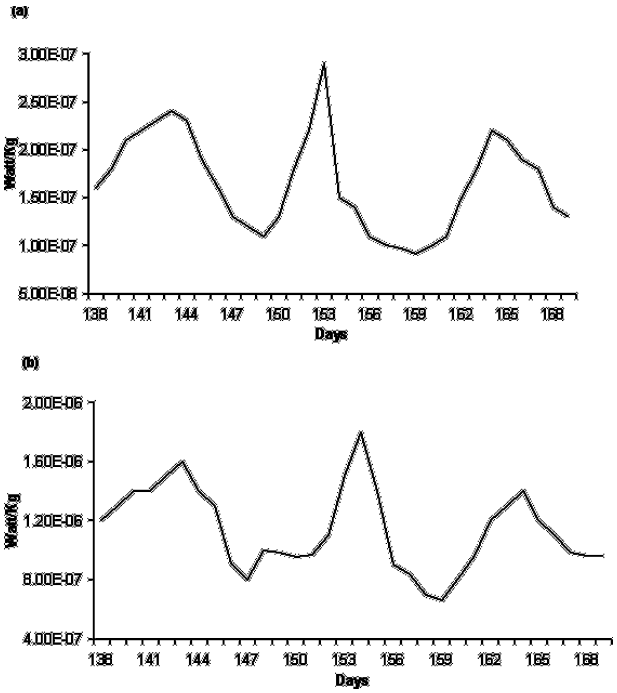

FIG. 3. (a) Nonlinear KE transfer to MJO in W kg^{-1} due to its interactions with the synoptic scales at 850 hPa within days 138–169 (i.e., 6 Jul–30 Sep 2001). (b) Same as (a) but for the contribution to MJO from all other time scales.

All possible triads for these interactions are included here. Figures 3a,b show the results for categories 1) and 2) above at the 850-hPa level and Figs. 4a,b show the same at the 1000-hPa level. These integrations involved with frequency cospectra and cross bispectra cover an average for all the spectral transform grid points (resolution T42) over a tropical belt (10°S–10°N, 60°–110°E). These computations of cospectra require only the time series of different functions at individual transferred grid points; thus, it is possible to examine these results over the Tropics.

Given a string of 364 days of data we can find the proportional contribution to the scale interactions from a single day. This follows a procedure we had previously followed (Krishnamurti et al. 2000). We take an initial n days of datasets (where n is of the order of 182). We use this n day string to calculate scale interactions in the frequency domain. We next increase this total string to $n + 1$ days and calculate the scale interactions. The difference in calculation of the $n + 1$ day string minus the n day string provides the contribution to the scale interactions from the dataset of day $n + 1$in detail. We increase n sequentially and repeat this process to evaluate the contributions for a number of sequential days.

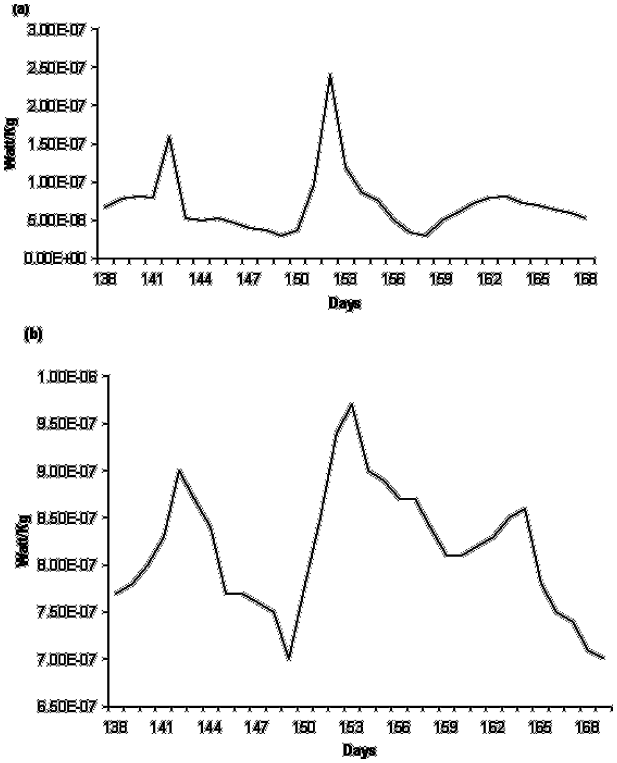

FIG. 4. Same as Fig. 3a but for 1000 hPa.

In Figs. 3a,b we show the results at 850 hPa from a part of the time series covering days 138–169 (which corresponds to 6 July–30 September 2001). Within this period, we were especially interested in day 153 (Fig. 1) when a sharp phase locking between the MJO and synoptic time scales was noticed. We note that on this day a distinct maxima in the energy transfer to the MJO time scale from all other possible time scales and especially the synoptic time scale was present. Two other minor maxima in the energy exchange were also noted for days 143 and 164. The primary maximum appears to be clearly related to the major phase-locking event. These secondary maxima, we call these side lobes, were also related to minor, short duration coherent phases between the MJO and the synoptic time scales.

The results at the 1000-hPa level (Figs. 4a,b) for the interactions of the MJO time scales with the synoptic time scales were equally striking showing a large transfer to the MJO time scale on day 153 when the phase locking was quite well marked. The same kind of result was also carried out in the kinetic energy exchanges when the interactions of the MJO time scale with all other possible frequencies were considered (at the 1000-hPa level). These also included the side lobes (i.e., the minor peaks of energy transfer on days 143 and 164).

5. Surface fluxes of moisture

The surface and PBL fluxes of moisture on certain time scales (e.g., the MJO) when it interacts with a pair of other permissible time scales were described by Eqs. (A3) and (A4), respectively. It was possible to include here the interaction of all time scales within the 30–60-day time frame with all other permissible pairs within 1–180 days. Computations following Krishnamurti et al. (2003) were carried out within the constant flux layer and the planetary boundary layer. Here (Fig. 5) we present a comparison of fluxes on the MJO time scale arising from its interactions with all other time scales for the surface layer and the PBL. These results are also compared with the total moisture fluxes (include all scales) obtained from the ECMWF operational data files. These fluxes are averaged values over a domain between 10°S–10°N and 60°–110°E. The time series presented here includes a major phase-locking episode that occurred near day 153. It was necessary to obtain daily contributions to the triad interactions and those were obtained by the same procedure as was outlined in the previous section. Here the start date of the display of the results in Fig. 5 is day 138, which corresponds to 1200 UTC 6 July 2001. We note an enhancement of moisture fluxes on day 153 when a pronounced phase locking was under way. There are two side lobes of secondary maxima around days 143 and 164 when minor phase-locking episodes were noted. Surprisingly the total fluxes of the ECMWF datasets (that must include all time scales in their totality) also exhibited these primary and the secondary flux maxima. This sug-

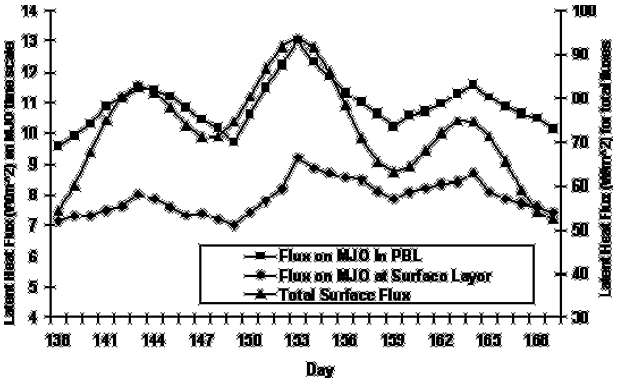

FIG. 5. Comparison of moisture fluxes (W m^{-2}) on the MJO time scale arising from its interactions with all other time scales for the surface layer and the PBL with the total fluxes obtained from the ECMWF operational data files. The ordinate scale for MJO time scale fluxes is on the left side of the diagram whereas for the total fluxes the scale is included in the right side of the diagram.

gests that our results of robust scale interactions during episodes of phase locking are revealed by the total fluxes as well. The mean fluxes at the top of the constant flux layer were around 7.7 W m^{-2} during the interaction of the MJO time scale with other time scales. The maximum value of this flux was as high as 8.4 W m^{-2} during phase locking. The corresponding values at the top of the PBL were 10.7 W m^{-2} for the mean value and 12.3 W m^{-2} for the maximum value. The total fluxes at the surface from the ECMWF data files had corresponding values of 76 W m^{-2} for the mean and 90 W m^{-2} for the maximum, which includes the totality of all scales. The ordinate scale for MJO time scale fluxes are presented on the left side of the diagram whereas for the total fluxes the scale is included on the right side of the diagram.

6. Concluding remarks

The approach of the present paper is one of the scale interactions in the frequency domain. In a recent study Krishnamurti et al. (2003) investigated the maintenance of the MJO on the 30–60-day time scale from a coupled atmosphere–ocean model simulation. In that study, the planetary boundary layer dynamics/thermodynamics of a coupled global model was utilized as the frame of reference. It was shown that the large growth of fluxes on the time scale of the MJO arose from nonlinear interactions of frequencies of the MJO time scale with a pair of frequencies on the synoptic scales of a 2–7 day period. That study also revealed some aspects on the tropospheric expanse of the MJO time scale via deep convection and related large planetary-scale divergent circulations. In the course of examining those aspects we noted that enhancements of the interactions among the MJO time scale and the synoptic time scale occurred during episodes of phase locking.

The present paper focuses on the issue of phase locking through nonlinear dynamics. The present study is based on the use of ECMWF Re-Analysis (ERA-40). We have used daily analysis covering datasets for year 2001, and examined here epochs of large growths of eddy kinetic energy and of moisture fluxes on the MJO time scale that seem to coincide with episodes of phase locking. In this study we have explored scale interactions among frequencies on the MJO time scale and the synoptic scales and their settings during phase locking for possible explanations of explosive growth of a time scale. Both the methodologies of inquiry in terms of energetics and PBL fluxes used here entail triple-product nonlinearities that are described by triad interactions. We first examined a time series of zonal winds at 850 hPa at a single location to illustrate the "in and out" of phase behavior of long and short time scales, which interact through nonlinear dynamics. We noticed occasional phase locking among this family of low- and high-frequency motions. In this study we have shown that nonlinear energy exchanges can amplify when phase locking occurs among families of waves on two disparate time scales.

We constructed a specialized diagram with the phase of one wave along the abscissa and the phase of a second wave along the ordinate. A principal diagonal (at 45° angle) of this diagram is a line of equal phase for the two frequencies. We set the phase of a third frequency identical to that of the second. In these instances the energy exchanges were seen to exhibit maximum values along the principal diagonal. The values of energy exchanges away from the principal diagonal were smaller where phases of low-frequency motions were different from each other. The results show that a salient term of the scale interactions among a triad of frequencies does seem to maximize the energy transfer to low-frequency motions (such as the MJO time scale) through its interaction with high frequencies (such as the synoptic time scales) when their phases are identical.

To illustrate the large growth of energy exchange for the MJO time scale as it interacts with a pair of frequencies on the synoptic time scale, with the added phase-locking caveat, we had to design a special computational phase. Using the complete kinetic to kinetic energy exchange equations we first performed these computations of scale interactions using 138 days of data. That provided a measure of the energy exchange from the synoptic scale to the MJO time scale, averaged over these 138 days. The data length was next increased to 139 days. The results of these exchanges from 139 days minus the exchange from 138 days provided us the contribution to those scale interactions from day 139. This exercise of incrementing one day at a time was sequentially extended to arrive at a time series of daily contributions. It is this dataset that revealed that the days of phase locking among triads of frequencies do seem to convey large kinetic energy exchanges and boundary layer fluxes as well.

Our, more complete, computations of kinetic energy exchanges at 850 and 1000 hPa cover days 138 to 169 of a time series (which corresponds to 6 July–30 September 2001). These show an interesting feature on day 153 when a sharp phase locking between the MJO and synoptic time scales was present. We noted that on this day a distinct maxima in the energy transfer to the MJO time scale from all other possible pairs of the time scale

and especially when the synoptic time scale was present. This event of maximum energy transfer appears to be related to the major phase-locking phenomenon. Two side lobes of secondary maxima of energy exchanges around days 143 and 164 were noted when minor phase-locking episodes occurred. Computations of moisture fluxes on the MJO time scale arising from interactions with all other time scales for the surface layer and the PBL also show an enhancement of moisture fluxes on day 153 when the pronounced phase locking was under way. Here, too, secondary maxima around days 143 and 164 due to minor phase-locking phenomena were noted. The results of the computations of the total fluxes of the ECMWF datasets, which include all time scales in their totality also revealed the occurrence of these primary and secondary flux maxima occurring on days 153, 143–164, respectively. This suggests the importance of nonlinear-scale interactions during episodes of phase locking for the amplification of MJO on the 30–60-day time scale.

This interpretation needs to be explored for other well-known phase-locking observations among several other possible time scales that have been mentioned in the literature.

Acknowledgments. The research work reported here was supported by NSF Grant ATM-0241517, INT-0302172, and NOAA Grants NA06GPO512 and NA16GP1365. The authors thank Drs. M. K. Biswas and T. S. V. Vijaya Kumar for their scientific discussions and for the assistance in improving the quality of this manuscript.

APPENDIX

Mathematical Formulation of the Kinetic Energy Problem in the Frequency Domain

Following Krishnamurti et al. (2000), the equation for nonlinear exchanges of kinetic energy among different frequencies r and s and a frequency n can be written as

$$\langle L(n)\rangle = \frac{1}{2}\left[\begin{array}{l} +\sum\limits_{r+s=n} \\ +\sum\limits_{r-s=n} \\ +\sum\limits_{r-s=-n} \end{array}\right] \mathrm{UOC}_n\mathrm{UTC}_r\left(2\frac{\partial \mathrm{UTC}_s}{\partial x}+\frac{\partial \mathrm{VTC}_s}{\partial y}+\frac{\partial \mathrm{WTC}_s}{\partial p}-\frac{\tan\phi}{a}\mathrm{VTC}_s\right)$$

$$+\mathrm{UOC}_n\left(\frac{\partial}{\partial y}\mathrm{UTC}_r\mathrm{VTC}_s+\frac{\partial}{\partial p}\mathrm{UTC}_r\mathrm{WTC}_s\right)+\mathrm{VOC}_n\mathrm{UTC}_r\left(\frac{\partial}{\partial x}\mathrm{VTC}_s-\frac{\tan\phi}{a}\mathrm{UTC}_s\right)$$

$$+\mathrm{VOC}_n\mathrm{VTC}_r\left(2\frac{\partial}{\partial y}\mathrm{VTC}_s+\frac{\partial}{\partial p}\mathrm{WTC}_s\right)+\mathrm{VOC}_n\left(\frac{\partial}{\partial x}\mathrm{UTC}_r\mathrm{VTC}_s+\frac{\partial}{\partial p}\mathrm{VTC}_r\mathrm{WTC}_s\right)$$

$$+\frac{1}{2}\left[\begin{array}{l} +\sum\limits_{r+s=n} \\ +\sum\limits_{r-s=n} \\ -\sum\limits_{r-s=-n} \end{array}\right] \mathrm{UOS}_n\mathrm{UTS}_r\left(2\frac{\partial \mathrm{UTC}_s}{\partial x}+\frac{\partial \mathrm{VTC}_s}{\partial y}+\frac{\partial \mathrm{WTC}_s}{\partial p}-\frac{\tan\phi}{a}\mathrm{VTC}_s\right)$$

$$+\mathrm{UOS}_n\left(\frac{\partial}{\partial y}\mathrm{UTS}_r\mathrm{VTC}_s+\frac{\partial}{\partial p}\mathrm{UTS}_r\mathrm{WTC}_s\right)+\mathrm{VOS}_n\mathrm{UTS}_r\left(\frac{\partial}{\partial x}\mathrm{VTC}_s-\frac{\tan\phi}{a}\mathrm{UTC}_s\right)$$

$$+\mathrm{VOS}_n\mathrm{VTS}_r\left(2\frac{\partial}{\partial y}\mathrm{VTC}_s+\frac{\partial}{\partial p}\mathrm{WTC}_s\right)+\mathrm{VOS}_n\left(\frac{\partial}{\partial x}\mathrm{UTS}_r\mathrm{VTC}_s+\frac{\partial}{\partial p}\mathrm{VTS}_r\mathrm{WTC}_s\right)$$

$$+\frac{1}{2}\begin{bmatrix}-\sum_{r+s=n}\\ +\sum_{r-s=n}\\ +\sum_{r-s=-n}\end{bmatrix}\mathrm{UOC}_n\mathrm{UTS}_r\left(2\frac{\partial \mathrm{UTS}_s}{\partial x}+\frac{\partial \mathrm{VTS}_s}{\partial y}+\frac{\partial WTS_s}{\partial p}-\frac{\tan\phi}{a}\mathrm{VTS}_s\right)$$

$$+\mathrm{UOC}_n\left(\frac{\partial}{\partial y}\mathrm{UTS}_r\mathrm{VTS}_s+\frac{\partial}{\partial p}\mathrm{UTS}_r\mathrm{WTS}_s\right)+\mathrm{VOC}_n\mathrm{UTS}_r\left(\frac{\partial}{\partial x}\mathrm{VTS}_s-\frac{\tan\phi}{a}\mathrm{UTS}_s\right)$$

$$+\mathrm{VOC}_n\mathrm{VTS}_r\left(2\frac{\partial}{\partial y}\mathrm{VTS}_s+\frac{\partial}{\partial p}\mathrm{WTS}_s\right)+\mathrm{VOC}_n\left(\frac{\partial}{\partial x}\mathrm{UTS}_r\mathrm{VTS}_s+\frac{\partial}{\partial p}\mathrm{VTS}_r\mathrm{WTS}_s\right)$$

$$+\frac{1}{2}\begin{bmatrix}+\sum_{r+s=n}\\ -\sum_{r-s=n}\\ +\sum_{r-s=-n}\end{bmatrix}\mathrm{UOS}_n\mathrm{UTC}_r\left[\left(2\frac{\partial \mathrm{UTS}_s}{\partial x}+\frac{\partial \mathrm{VTS}_s}{\partial y}+\frac{\partial \mathrm{WTS}_s}{\partial p}-\frac{\tan\phi}{a}\right)\mathrm{VTS}_s\right]$$

$$+\mathrm{UOS}_n\left(\frac{\partial}{\partial y}\mathrm{UTC}_r\mathrm{VTS}_s+\frac{\partial}{\partial p}\mathrm{UTC}_r\mathrm{WTS}_s\right)+\mathrm{VOS}_n\mathrm{UTC}_r\left(\frac{\partial}{\partial x}\mathrm{VTS}_s-\frac{\tan\phi}{a}\mathrm{UTS}_s\right)$$

$$+\mathrm{VOS}_n\mathrm{VTC}_r\left(2\frac{\partial}{\partial y}\mathrm{VTS}_s+\frac{\partial}{\partial p}\mathrm{WTS}_s\right)+\mathrm{VOS}_n\left(\frac{\partial}{\partial x}\mathrm{UTC}_r\mathrm{VTS}_s+\frac{\partial}{\partial p}\mathrm{VTC}_r\mathrm{WTS}_s\right). \quad \text{(A1)}$$

where a is the earth's radius, ϕ is the latitude, and n, r, and s are the frequency indices. Here (UOC, UOS), (VOC, VOS) are the temporal Fourier cosine and sine coefficients of the observed u, v fields associated with frequency, n, whereas (UTC, UTS), (VTC, VTS), and (WTC, WTS) are the same except for transient u, v, and w fields associated with frequencies r and s. Most of these terms involve triple products. A detailed derivation of the above relation can be found in Hayashi (1980)and Krishnamurti et al. (2000).

Mathematical formulation of the surface layer/PBL flux problem in the frequency domain

We shall also examine the scale interaction problem within the boundary layer physics and show that similar nonlinearities are present there as well. The basic equations used for computation of surface fluxes are based on the work of Businger et al. (1971). The surface similarity theory, which can be expressed following Krishnamurti et al. (1998), is

$$F = \eta C|V_a|(Q_a - Q_s), \quad \text{(A2)}$$

where η is a constant, C is a stability-dependent exchange coefficient from the surface similarity theory, $|V_a|$ is the surface wind speed, and Q_s are the values for any flux variable at the anemometer level and the surface level, respectively. In Krishnamurti et al. (2003) we viewed this as a triple product among C, $|V_a|$, and $(Q_a - Q_s)$ Following the same paper the final expression of latent heat fluxes in the frequency domain is given as

$$\langle L_h(n)\rangle = \frac{\rho}{2}\begin{bmatrix}+\sum_{r+s=n}\\ +\sum_{r-s=n}\\ +\sum_{r-s=-n}\end{bmatrix}[\mathrm{LHC}(n)\times\mathrm{MVC}(r)\times\mathrm{DMC}(s)]+\frac{\rho}{2}\begin{bmatrix}-\sum_{r+s=n}\\ +\sum_{r-s=n}\\ +\sum_{r-s=-n}\end{bmatrix}[\mathrm{LHC}(n)\times\mathrm{MVS}(r)\times\mathrm{DMS}(s)]$$

$$+\frac{\rho}{2}\begin{bmatrix}+\sum\limits_{r+s=n}\\-\sum\limits_{r-s=n}\\+\sum\limits_{r-s=-n}\end{bmatrix}[\mathrm{LHS}(n)\times\mathrm{MVC}(r)\times\mathrm{DMS}(s)]0+\frac{\rho}{2}\begin{bmatrix}+\sum\limits_{r+s=n}\\+\sum\limits_{r-s=n}\\-\sum\limits_{r-s=-n}\end{bmatrix}[\mathrm{LHS}(n)\times\mathrm{MVS}(r)\times\mathrm{DMC}(s)]. \quad \text{(A3)}$$

where ρ is the density of air. Here (LHC, LHS), (MVC, MVS), and (DMC, DMS) are the cosine and sine coefficients of C, $|V|$, and $(Q_s - Q_a)$ associated with frequencies n, r, and s, respectively. This formulation essentially follows Krishnamurti et al. (2003). The time series of these variables were subjected to the Hayashi (1980) cospectral method. This was centered on the MJO time scale of 30–50 days. We examined the gain or loss of surface fluxes on the MJO time scale as it interacted with any other pair of time scales.

A similar triple product can also be seen in the formulation of the planetary boundary layer, which is essentially a diffusive approach. This is based on K theory, where the exchange coefficient is a function of the Richardson number and mixing length theory used by Blackadar (1962) and Louis (1979). The final expression of this formulation includes a triple product of $\mathrm{Ri}_{i\beta}\partial q/\partial z$ and $\partial|V|/\partial z$. Following Krishnamurti et al. (2003) the moisture flux is given as

$$\begin{aligned}\langle F_Q(n)\rangle = {}& \frac{\rho C_p}{2}\frac{\kappa^2 z^2}{(1+\kappa z/\lambda)^2}\begin{bmatrix}+\sum\limits_{r+s=n}\\+\sum\limits_{r-s=n}\\+\sum\limits_{r-s=-n}\end{bmatrix}[\mathrm{RIC}(n)\times\mathrm{PQC}(r)\times\mathrm{VTC}(s)]\\ &+\frac{\rho C_p}{2}\frac{\kappa^2 z^2}{(1+\kappa z/\lambda)^2}\begin{bmatrix}-\sum\limits_{r+s=n}\\+\sum\limits_{r-s=n}\\+\sum\limits_{r-s=-n}\end{bmatrix}[\mathrm{RIC}(n)\times\mathrm{PQS}(r)\times\mathrm{VTS}(s)]\\ &+\frac{\rho C_p}{2}\frac{\kappa^2 z^2}{(1+\kappa z/\lambda)^2}\begin{bmatrix}+\sum\limits_{r+s=n}\\-\sum\limits_{r-s=n}\\+\sum\limits_{r-s=-n}\end{bmatrix}[\mathrm{RIS}(n)\times\mathrm{PQC}(r)\times\mathrm{VTS}(s)]\\ &+\frac{\rho C_p}{2}\frac{\kappa^2 z^2}{(1+\kappa z/\lambda)^2}\begin{bmatrix}+\sum\limits_{r+s=n}\\+\sum\limits_{r-s=n}\\-\sum\limits_{r-s=-n}\end{bmatrix}[\mathrm{RIS}(n)\times\mathrm{PQS}(r)\times\mathrm{VTC}(s)]. \end{aligned} \quad \text{(A4)}$$

where (RIC, RIS), (PQC, PQS), and (VTC, VTS) are the cosine and sine coefficients of the terms involving $\mathrm{Ri}_{i\beta}$, $\partial q/\partial z$, and $\partial|V|/\partial z$ associated with frequencies n, r, and s, respectively. Here κ is the von Kármán constant, z is the height of the relevant computational level in the in the PBL, and λ is a constant that denotes an asymptotic mixing length whose value for moisture fluxes is set to 450 m.

REFERENCES

An, S.-I., and B. Wang, 2001: Mechanisms of locking of the El Niño and La Niña mature phases to boreal winter. *J. Climate,* **14,** 2164–2176.

——, and F.-F. Jin, 2004: Nonlinearity and asymmetry of ENSO. *J. Climate,* **17,** 2399–2412.

Blackadar, A. K., 1962: The vertical distribution of wind and turbulent exchange in a neutral atmosphere. *J. Geophys. Res.,* **67,** 3095–3102.

Businger, J. A., J. C. Wyngard, Y. Izumi, and E. F. Bradley, 1971: Flux profile relationship in the atmospheric surface layer. *J. Atmos. Sci.,* **28,** 181–189.

Cane, M. A., and S. E. Zebiak, 1985: A theory for El Niño and the Southern Oscillation. *Science,* **228,** 1084–1087.

Chakraborty, D. R., and N. K. Agarwal, 1996: Role of triad kinetic energy interactions for maintenance of upper tropospheric low frequency waves during summer monsoon 1998. *Adv. Atmos. Sci.,* **13,** 91–102.

Hayashi, Y., 1980: Estimation of nonlinear energy transfer spectra by the cross-spectral method. *J. Atmos. Sci.,* **37,** 299–307.

Kim, K.-Y., 2002: Investigation of ENSO variability using cyclostationary EOFs of observational data. *Meteor. Atmos. Phys.,* **81,** 149–168.

Krishnamurti, T. N., H. S. Bedi, and V. M. Hardiker, 1998: *An Introduction to Global Spectral Modeling.* Oxford University Press, 253 pp.

——, D. Bachiochi, T. Larow, B. Jha, M. Tewari, D. R. Chakraborty, R. Correa-Torres, and D. Oosterhof, 2000: Coupled atmosphere–ocean modeling of the El Niño of 1997–98. *J. Climate,* **13,** 2428–2459.

——, D. R. Chakraborty, N. Cubukcu, L. Stefanova, and T. S. V. Vijaya Kumar, 2003: A mechanism of the Madden–Julian Oscillation based on interactions in the frequency domain. *Quart. J. Roy. Meteor. Soc.,* **129,** 2559–2590.

Louis, J. F., 1979: A parametric model of vertical eddy fluxes in the atmosphere. *Bound.-Layer Meteor.,* **17,** 187–202.

Neelin, J. D., F.-F. Jin, and H.-H. Syu, 2000: Variations in ENSO phase-locking. *J. Climate,* **13,** 2570–2590.

Philander, S. G. H., T. Yamagata, and R. C. Pacanowski, 1984: Unstable air–sea interactions in the Tropics. *J. Atmos. Sci.,* **41,** 604–613.

Sheng, J., and Y. Hayashi, 1990a: Observed and simulated energy cycles in the frequency domain. *J. Atmos. Sci.,* **47,** 1243–1254.

——, and ——, 1990b: Estimation of atmospheric energetics in the frequency in the FGGE year. *J. Atmos. Sci.,* **47,** 1255–1268.

Ueda, H., 2002: Equatorial monsoon system as regulation for a dipole mode in the Indian Ocean. *Pap. Meteor. Geophys.,* **51,** 147–154.

Wang, B., and X. Xu, 1997: Northern Hemisphere summer monsoon singularities and climatological intraseasonal oscillation. *J. Climate,* **10,** 1071–1085.